J Solid State Electrochem (2012) 16:1055–1065
DOI 10.1007/s10008-011-1492-7

ORIGINAL PAPER

Effects of molecular weight, heating rate, synthetic temperature and sintering duration on electrochemical properties of a $LiFePO_4$/C cathode material pyrolyzed from lithium polyacrylate

Kerun Yang · Xuebu Hu · Yongjian Huai · Zhongqi Shi · Zhenghua Deng · Jishuan Suo

Received: 25 May 2011 / Revised: 22 June 2011 / Accepted: 26 June 2011 / Published online: 12 July 2011

Abstract A $LiFePO_4$/C composite was obtained by a polymer pyrolysis reduction method, using lithium polyacrylate (LiPAA) as carbon source and fractional lithium source, and $FePO_4 \cdot 2H_2O$ as iron and phosphorus source. The structure of the $LiFePO_4$/C composites was investigated by X-ray diffraction (XRD). The micromorphology of the precursors and $LiFePO_4$/C powders was observed using scanning electron microscopy (SEM). Laser particle analyzer and BET were also used to characterize the materials. It was found that the micromorphology, particle size distribution and specific surface area of $LiFePO_4$/C composites were greatly influenced by the molecular weight of LiPAA. The electrochemical properties of the $LiFePO_4$/C composites were evaluated by cyclic voltammograms (CVs), electrochemical impedance spectra (EIS) and constant current charge/discharge cycling tests. The results showed that the molecular weight of LiPAA, heating rate, synthetic temperature and sintering duration directly affected the electrochemical properties of $LiFePO_4$/C composites. The sample with the optimized electrochemical properties were obtained in the following conditions, i.e., LiPAA with the molecular weight of 20,000, heating rate of 10 °C min^{-1}, synthetic temperature of 700 °C and sintering duration of 15 h.

Keywords Lithium iron phosphate · Lithium polyacrylate · Molecular weight

K. Yang · Z. Shi · Z. Deng · J. Suo
Chengdu Institute of Organic Chemistry,
Chinese Academy of Sciences,
Chengdu, Sichuan 610041, China

K. Yang · Z. Shi · Z. Deng (✉) · J. Suo
Graduate School of Chinese Academy of Sciences,
Beijing, 100039, China
e-mail: zhdeng@cioc.ac.cn

X. Hu
Department of Chemistry and Materials,
Sichuan Normal University,
Chengdu, Sichuan 610066, China

Y. Huai
China Aviation Lithium Battery,
Luoyang, Henan 471003, China

Introduction

Olivine-type $LiFePO_4$ has attracted a great deal of interest as a cathode material for lithium-based secondary batteries because of its numerous appealing features, such as high theoretical capacity of 170 mAh g^{-1}, high safety, non-toxicity, a flat discharge voltage, and low cost [1–8]. However, $LiFePO_4$ suffers from low ionic transport rate and electronic conductivity. Recently, tremendous efforts have been made to overcome the ionic transport and electronic conductivity limitations, which include: (1) doping $LiFePO_4$ with foreign atoms [9–11]. Although this method can increase the conductivity to some degree [10], introducing guest atoms into the crystal lattices of $LiFePO_4$ may also be deleterious if it occurs on the lithium sites [12]. (2) Surface coating or admixing with electronically conductive materials (carbon [13–19], Ag [20] and conducting polymers [21–24]) has also been studied. (3) Decreasing the particle size may also improve the ionic transport issues [25–27], because reducing the particle size can significantly shorten the diffusion time of Li^+ in $LiFePO_4$, resulting in a

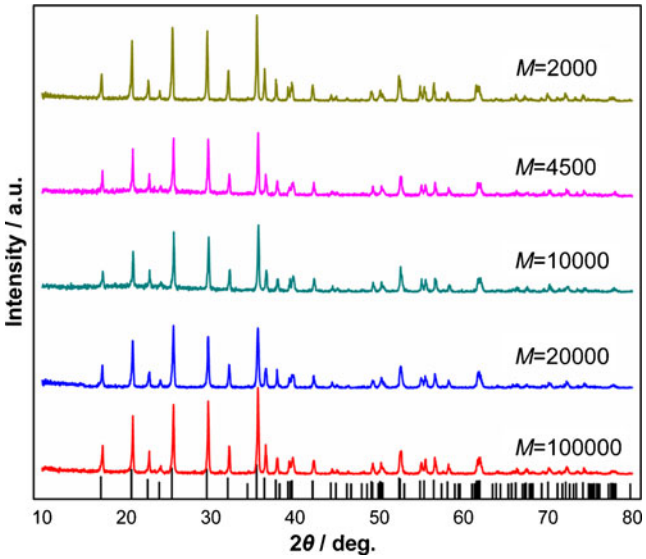

Fig. 1 XRD patterns of $LiFePO_4$/C composites derived from LiPAA with different molecular weight

much enhanced power performance. From these technologies, surface carbon coating has been widely used for improving the electronic conductivity of $LiFePO_4$.

However, previous studies [28–31] mainly focused on the synthesis of $LiFePO_4$/C composite materials by adding adscititious carbon source. In this work, $LiFePO_4$/C composite was synthesized from LiPAA and $FePO_4{\cdot}2H_2O$ by polymer pyrolysis reduction method without adscititious carbon source. Here, LiPAA was proposed to carbon source, reductant and fractional lithium source to prepare $LiFePO_4$/C composite. It is favorable to mix well and obtain homogenous $LiFePO_4$/C samples because no extra carbon source is added.

In previous work, we have prepared $LiFePO_4$/C composite by a polymer pyrolysis reduction method [32]. In the preparation process, we found that the molecular weight of LiPAA play important roles in determining the physical and electrochemical properties of $LiFePO_4$ cathode materials. Hence, in this study, the effects of molecular weight (mol. wt.) on the physical and electrochemical properties of $LiFePO_4$/C composite were investigated for the first time. Heating rates, synthetic temperatures and sintering durations were also examined.

Experimental

Synthesis of the $LiFePO_4$/C composite

The $LiFePO_4$/C composite was prepared using $Li_2C_2O_4$, $FePO_4{\cdot}2H_2O$, $H_2C_2O_4{\cdot}2H_2O$, and lithium polyacrylate (LiPAA, M=2,000, 4,500, 10,000, 20,000, 100,000) as the raw materials. $FePO_4{\cdot}2H_2O$, $Li_2C_2O_4$ and LiPAA ($Li_2C_2O_4$:LiPAA=1:2, according to the molar ratio) were dissolved in de-ionized water, and then a small quantity of $H_2C_2O_4{\cdot}2H_2O$ was added to the solutions to adjust the system to neutrality or slight acidity (pH=5–7). The above solution was thoroughly mixed by ball-milling in a planetary QM-3SP2 mill for 6 h. The homogeneous slurry was dried at 120 °C for 6 h to obtain the precursor. The precursors were sintered at 600–800 °C for 9–21 h in a flowing nitrogen with heating rate of 5–25 °C min^{-1}, followed by cooling to ambient temperature. The final powders were obtained by grinding.

Characterization of the precursor and $LiFePO_4$/C composite

The crystallographic structural characterization was performed by X-ray powder diffraction. X-ray diffraction (XRD) of the $LiFePO_4$/C composites was carried out on a Philips X′ Pert diffractometer equipped with Cu Kα radiation of λ=0.15418 nm in the range of $10°<2\theta<80°$. The micromorphology of the precursors and $LiFePO_4$/C composites was observed using an Impect F (FEI Company) scanning electron microscopy. The particle size (D_{50}) of the $LiFePO_4$/C composites was obtained from BT-9300H laser particle analyzer. The specific surface area of the samples was measured by nitrogen adsorption/desorption at −196 °C using a Builder SSA-4200 apparatus, and carbon content was detected using a Carlo Erba 1106 elemental analyzer (Italy).

Electrochemical measurements

Electrochemical measurements of the $LiFePO_4$/C composites were accomplished by assembling CR2032 coin cells. The electrodes were made by dispersing the $LiFePO_4$/C composites, super-p carbon black and an aqueous binder

Table 1 The lattice parameters of the $LiFePO_4$/C composites derived from LiPAA with different molecular weight

Sample ID	a (Å)	b (Å)	c (Å)	Cell volume (Å^3)
M=2,000	10.35986	6.0287	4.70901	294.11
M=4,500	10.34221	6.01332	4.69322	291.88
M=10,000	10.33671	6.00819	4.69413	291.53
M=20,000	10.34182	6.01329	4.69733	292.12
M=100,000	10.33758	6.01525	4.69907	292.2
PDF=83-2092	10.334	6.01	4.693	291.47

Table 2 Powder properties of the $LiFePO_4$/C composites derived from LiPAA with different molecular weight

Sample ID	Carbon content (%)	Surface area ($m^2\ g^{-1}$)	Particle size D_{50} (μm)
M=2,000	3.69	15.584	2.27
M=4,500	3.81	18.881	2.37
M=10,000	3.79	20.349	2.13
M=20,000	4.11	24.723	1.86
M=100,000	3.37	13.474	3.15

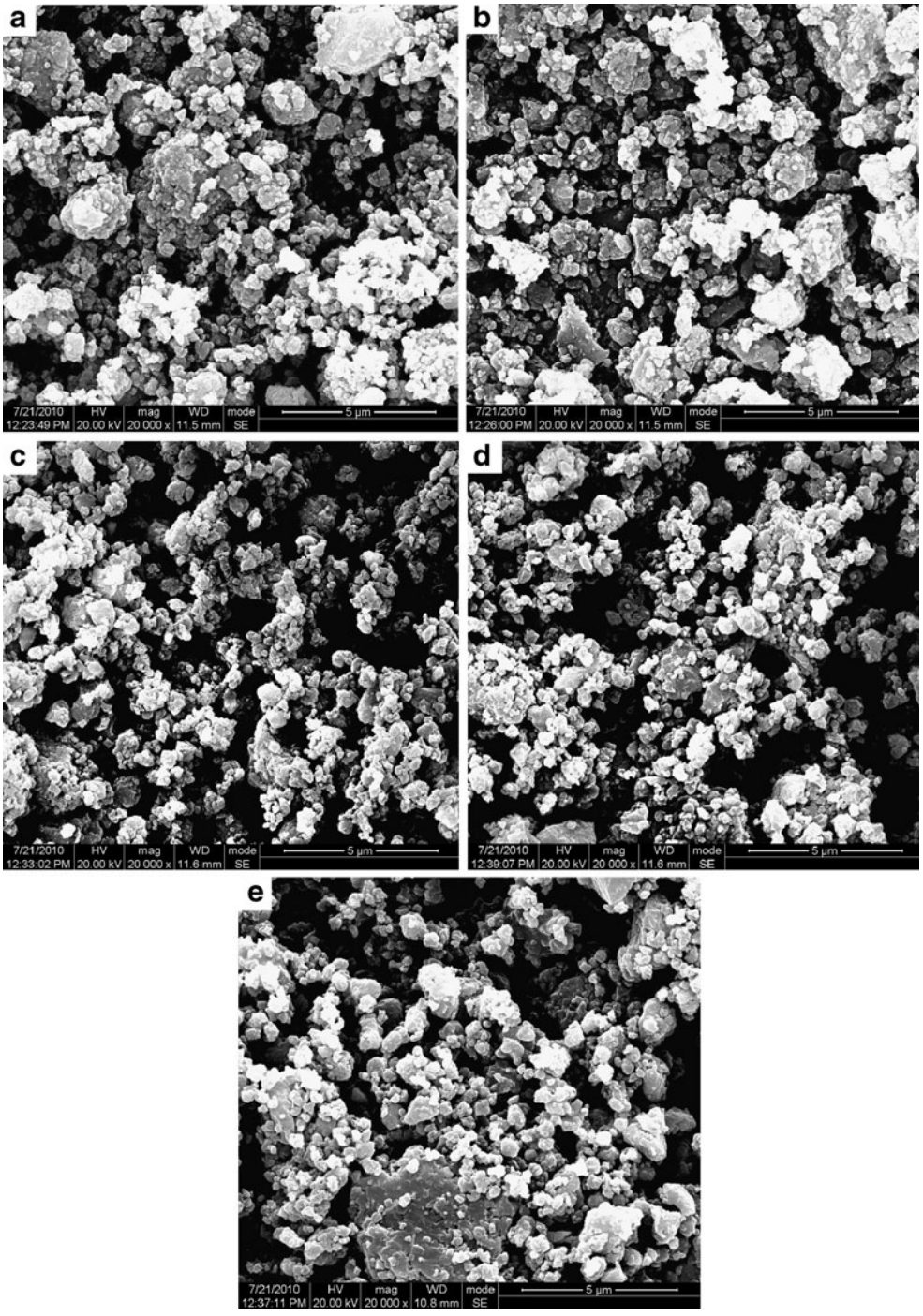

Fig. 2 SEM images of precursors containing LiPAA with different molecular weight: **a** 2,000, **b** 4,500, **c** 10,000, **d** 20,000, **e** 100,000

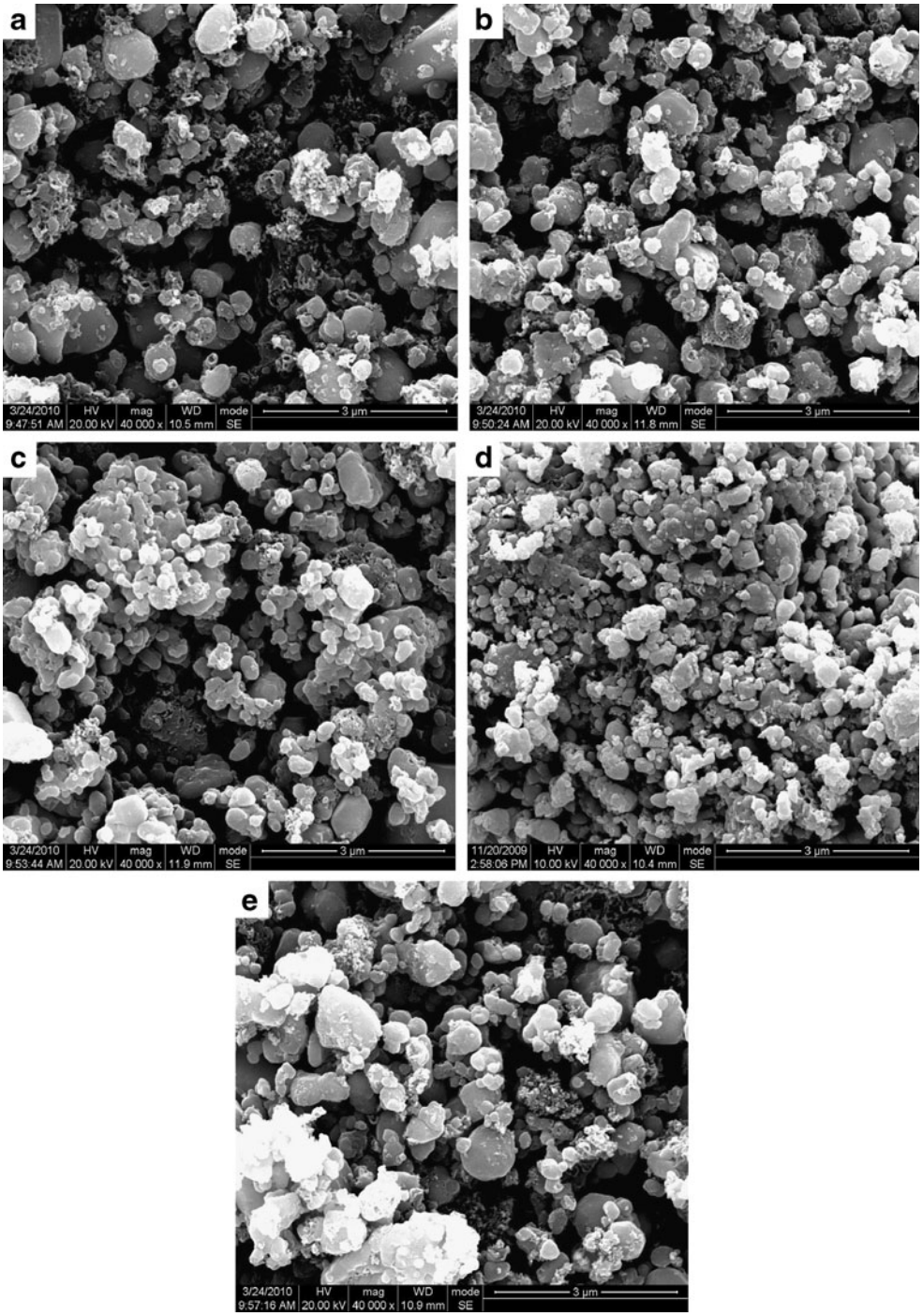

Fig. 3 SEM images of $LiFePO_4$/C composites derived from LiPAA with different molecular weight: **a** 2,000, **b** 4,500, **c** 10,000, **d** 20,000, **e** 100,000

LA132 (Indigo, China) homogeneously in a weight ratio of 80:10:10, casting the mixture uniformly onto an aluminum foil and drying at 100 °C. All electrodes were punched in the form of a disk with a diameter of 14.5 mm (area= 1.65 cm^2), pressed, dried at 100 °C under vacuum for 8 h, and then weighed to determine the active mass. A typical electrode disk contained 4–5 mg cm^{-2} of $LiFePO_4$/C active material with a thickness of 350–400 μm when coated on aluminum foil.

The electrochemical performances of the $LiFePO_4$/C composites were evaluated with a lithium metal foil as the counterelectrode and Celguard 2400 as the separator. The cell assembly was carried out in an argon-filled dry box. The electrolyte used was a 1 mol L^{-1} $LiPF_6$ solution in a mixture of ethylene carbonate, dimethyl carbonate and ethylene methyl carbonate (1:1:1 by volume). The cell was tested on a Neware Battery Tester (China) between 2.5 and 4.3 V, using a constant current charge/discharge mode. Cyclic voltamme-

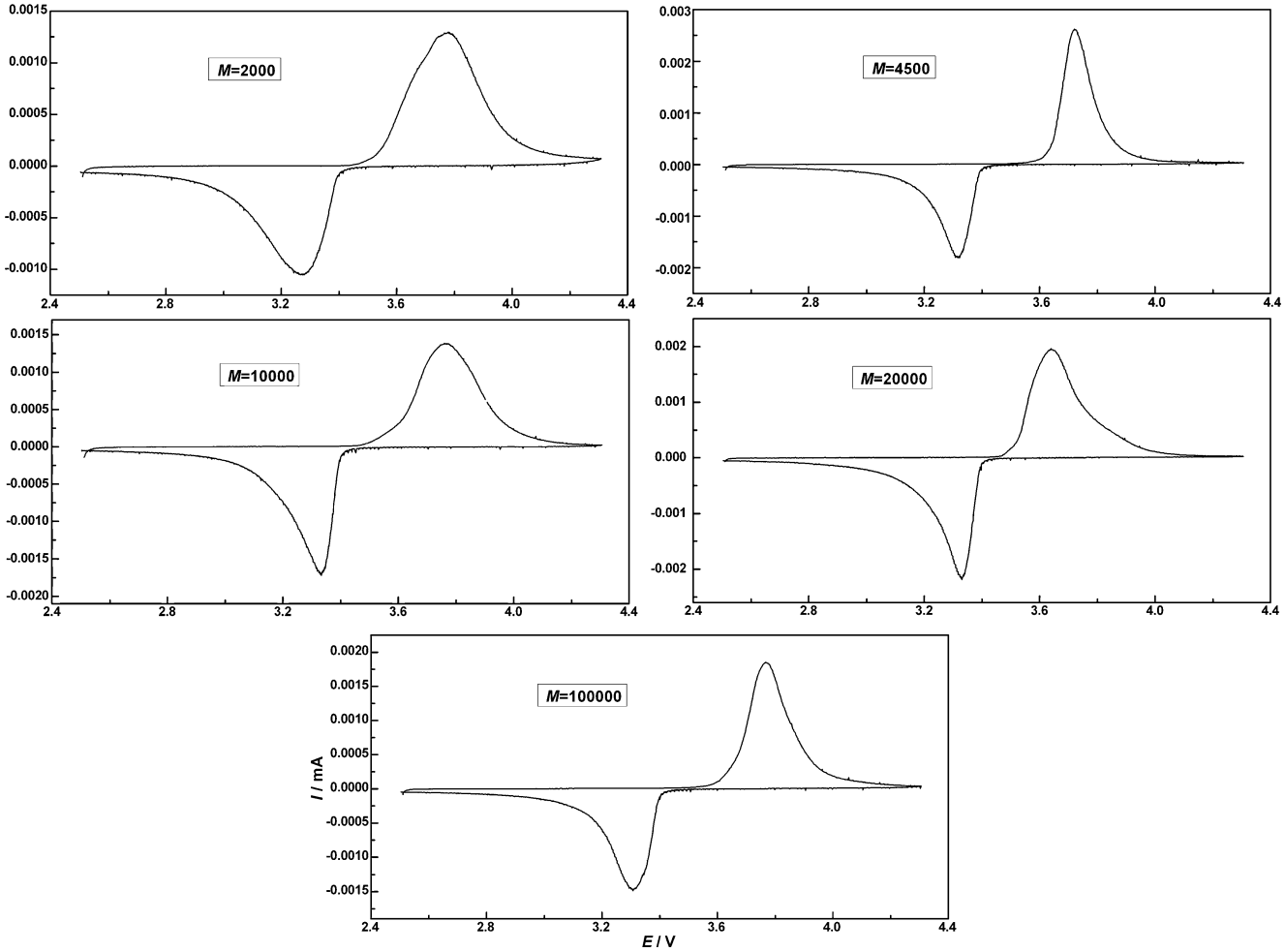

Fig. 4 First CVs of $LiFePO_4$/C composites from different molecular weight LiPAA

try measurements were performed using an Arbin Instrument (USA) at a scan rate of 0.1 mV s^{-1} between 2.5 and 4.3 V (vs. Li/Li^+). Electrochemical impedance spectra were measured by using a Solatron 1260 Impedance Analyzer in the frequency range 0.1–10^6 Hz at the open circuit with an ac voltage signal of 5 mV. Alltests were performed at room temperature without specially pointing out.

Results and discussion

Figure 1 shows the XRD patterns of as-prepared $LiFePO_4$/C composites sintered at 700 °C for 15 h under heating rate of 10 °C min^{-1} and LiPAA with different molecular weights (unless otherwise specified, the following samples were prepared under this condition). The XRD patterns reveal that all the samples are single phase of $LiFePO_4$ which can be indexed to the orthorhombic olivine type structure (JCPDS file no. 83-2092). It is found that no impurities exist in the XRD patterns, suggesting that the carbon derived from the LiPAA can effectively prevent the appearance of impurity phase during the heat treatment. The lattice parameters of $LiFePO_4$/C composites are listed in Table 1. It is shown that the lattice constants of all samples are approximately similar, indicating that the addition of LiPAA as carbon source has no obvious effect on the crystal structure of $LiFePO_4$ itself. There is no obvious diffraction response of the carbon because of its low content or amorphous state. The carbon content of all samples is listed in Table 2. From Fig. 1, we can also see that when the mol. wt. of LiPAA are 4,500, 10,000 and 20,000, the peak intensities of $LiFePO_4$ are almost identical, but when the LiPAA with mol. wt. of 2,000 and 100,000, the peak intensities of $LiFePO_4$ obviously increase compared with other samples. This indicates that too small (e.g., 2,000) or too large (e.g., 100,000) mol. wt. of LiPAA is propitious to increase the crystallization degree of the $LiFePO_4$/C composite.

Figure 2 presents the SEM images of the precursors containing LiPAA with different mol. wt. It can be observed

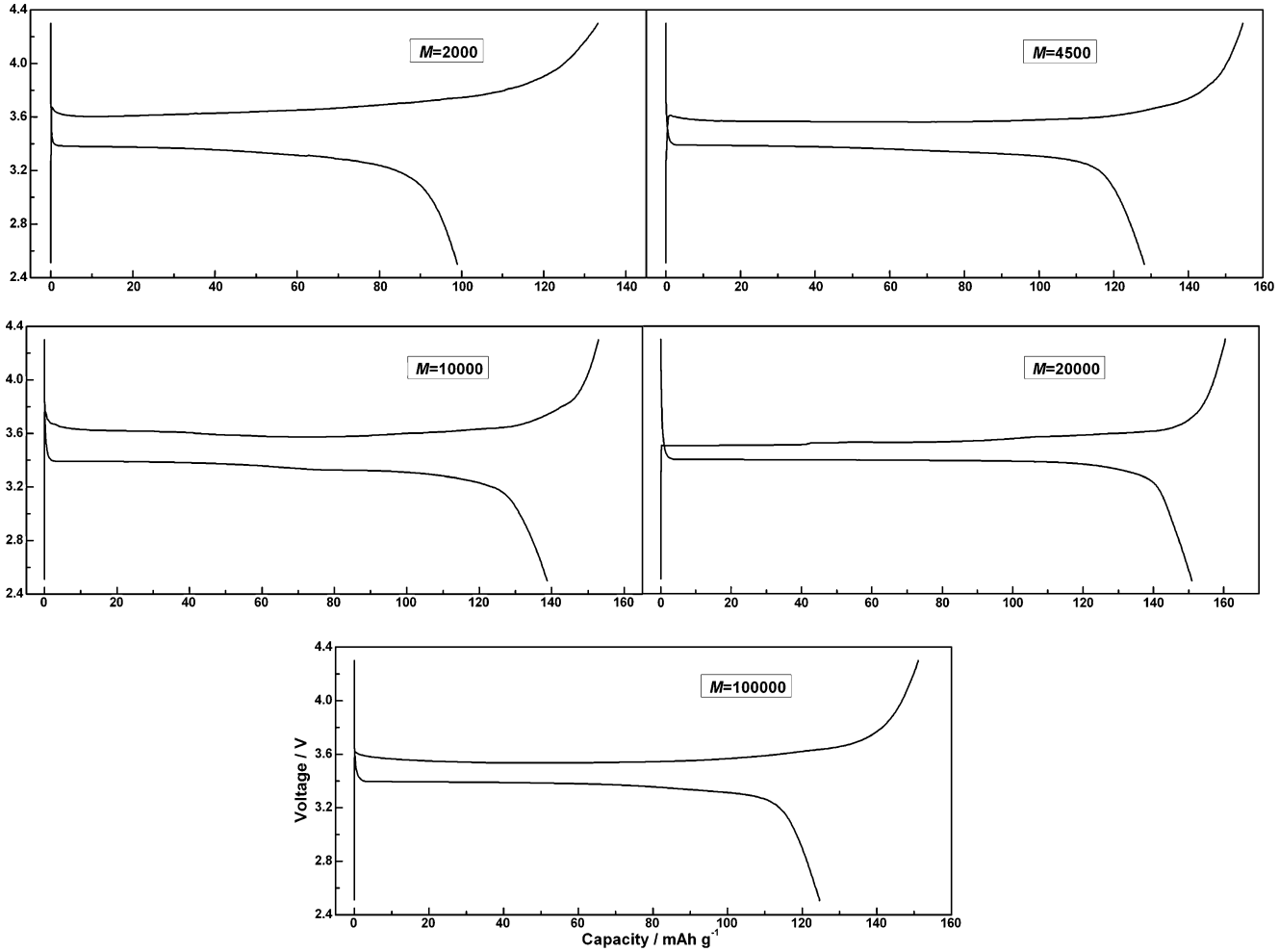

Fig. 5 Initial charge/discharge curves of $LiFePO_4$/C composites derived from LiPAA with different molecular weight at a rate of 0.2 C

that a good uniformity in size distribution is achieved when the mol. wt. of LiPAA are 10,000 and 20,000, whereas the precursors are bad dispersion and even serious aggregation when the mol. wt. of LiPAA are 2,000, 4,500 and 100,000.

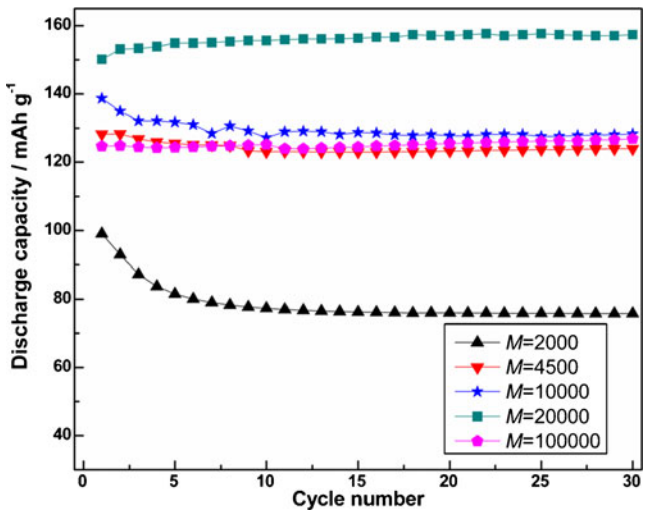

Fig. 6 Cycling performances of $LiFePO_4$/C composites derived from LiPAA with different molecular weight at a rate of 0.2 C

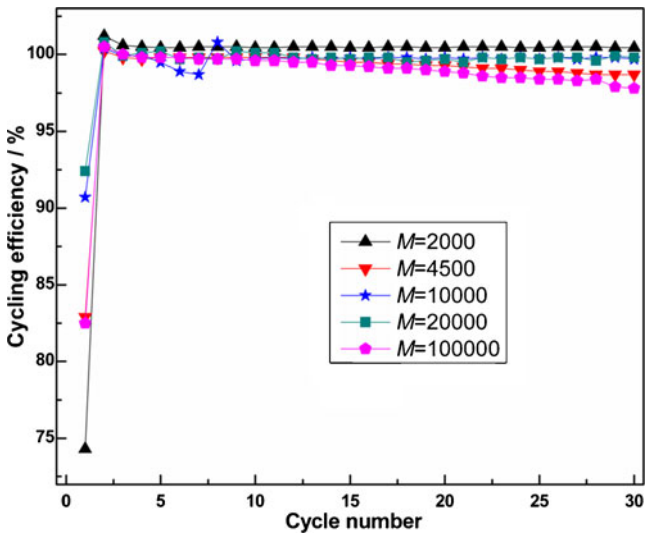

Fig. 7 Cycling efficiencies of $LiFePO_4$/C composites derived from LiPAA with different molecular weight at a rate of 0.2 C

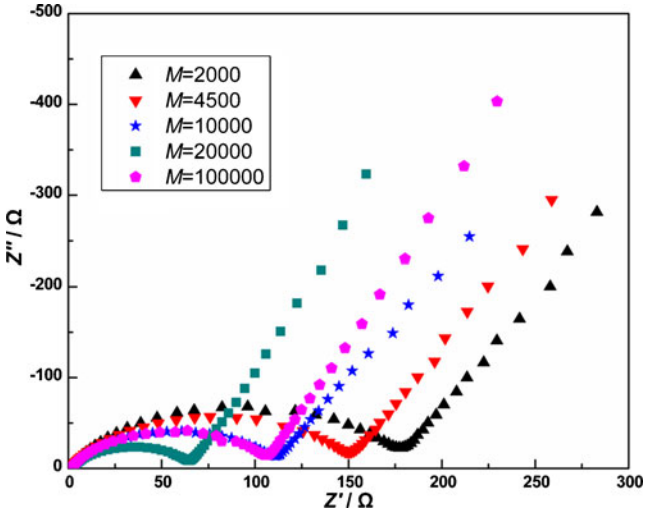

Fig. 8 Electrochemical impedance spectra of $LiFePO_4$/C composites from LiPAA with different molecular weight

The results can be attributed to the effect of molecular chain. When the mol. wt. of LiPAA is too small (e.g., 2,000 or 4,500), the circumvolute effect among molecular chains is too weak to prevent sedimentation of the precursor during drying. However, when the mol. wt. of LiPAA is too large (e.g., 100,000), the circumvolute effect among molecular chains is too strong to avoid aggregation of the precursor. Therefore, only when the mol. wt. of LiPAA is moderate (e.g., 10,000 or 20,000) can the precursors with uniform size distribution be obtained. The dispersion uniformity of the precursor directly affected the particle size distribution of final sample. The SEM images of as-prepared $LiFePO_4$/C composites are illustrated in Fig. 3. It can be seen that the samples show fine particle size distribution when the mol. wt. of LiPAA was 10,000 (Fig. 3c) and 20,000 (Fig. 3d). Otherwise, as shown in Fig. 3a, b, e, the samples has bad particle size distribution. And the particle size has a slight increase when LiPAA with mol. wt. of 2,000, 4,500 and 100,000 was used. It also can be observed that the samples derived from LiPAA with mol. wt of 10,000 and 20,000 have plenty of nano-sized microstructure on the surface of the particles, and the samples derived from LiPAA with mol. wt of 2,000, 4,500 and 100,000 show a comparatively glossy surface. The data from the BET measurement and laser particle analyzer is shown in Table 2. The $LiFePO_4$/C composites derived from LiPAA with mol. wt of 10,000 and 20,000 have larger specific surface area and smaller particle size (D_{50}) than the other samples, which is in good agreement with Fig. 3.

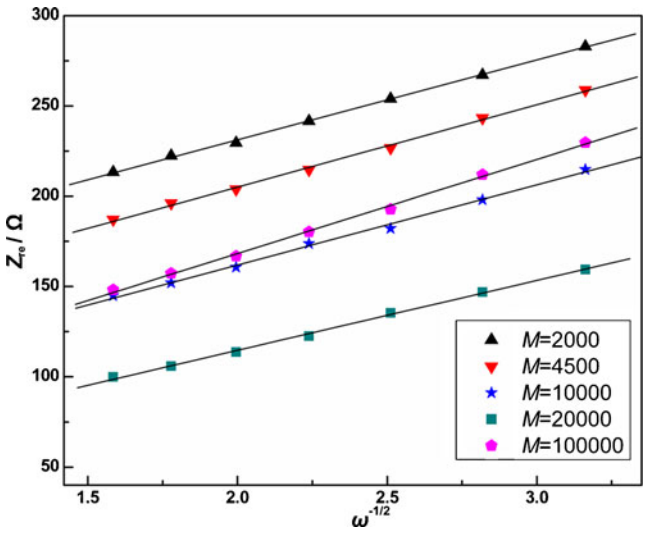

Fig. 9 The relationship plot between Z_{re} and $\omega^{-1/2}$ at low-frequency region

Figure 4 shows the first cyclic voltammograms (CVs) of the $LiFePO_4$/C composites. As shown in Fig. 4, a single pair of well-defined redox peaks is observed for all the samples. It suggested that there were no impurities in the composites, corresponding with the XRD patterns. The anodic and cathodic peaks correspond to the two-phase charge–discharge reaction of the Fe^{2+}/Fe^{3+} redox couple. The voltage separation (ΔV) between the anodic and the cathodic peaks are 0.49, 0.41, 0.43, 0.31 and 0.45 V for the LiPAA with mol. wt. of 2,000, 4,500, 10,000, 20,000 and 100,000, respectively, and the discharge peak currents decrease according to the order 20,000, 4,500, 10,000, 100,000, 2,000. This indicates that the sample derived from LiPAA with mol. wt. of 20,000 has lowest polarization, and the sample derived from LiPAA with mol. wt. of 2,000 has highest polarization.

The initial charge/discharge curves of as-prepared $LiFePO_4$/C composites are illustrated in Fig. 5. It is found that the discharge capacities of $LiFePO_4$ powders derived from LiPAA with mol. wt. of 2,000, 4,500, 10,000, 20,000 and 100,000 are 99, 128, 138, 151 and 125 mAh g^{-1}, respectively. The coulomb efficiencies of $LiFePO_4$/C composites decrease according to order 20,000, 10,000, 4,500, 100,000, 2,000. The highest discharge capacity and coulomb efficiency for the sample derived from LiPAA with mol. wt. of 20,000 can be explained in terms of fine particle size, low polarization and resistance.

The cycle performance of all samples at a rate of 0.2 C is shown in Fig. 6. It can be seen that the discharge capacity of the sample derived from LiPAA with mol. wt. of 20,000 gradually increase with the number of cycling, but the discharge capacity of the sample derived from LiPAA with mol. wt. of 2,000 quickly decrease, and the discharge capacities of the samples derived from LiPAA with mol. wt. of 4,500 and 10,000 decreased slightly, and the discharge capacity of the sample derived from LiPAA with mol. wt. of 100,000 shows very little increase. The capacity retentions are 76.6%, 96.7%, 92.5%, 104.1% and 101.8% for the samples derived from LiPAA with mol. wt. of 2,000, 4,500, 10,000, 20,000 and 100,000, respectively, after 20 cycles.

Table 3 The impedance parameters of the $LiFePO_4$/C cells

Sample ID	R_e (Ω)	R_{ct} (Ω)	σ(Ω cm $S^{-1/2}$)	D (cm^2 S^{-1})	i (mA cm^{-2})
M=2,000	1.94	179	44.1	1.13×10^{-13}	1.43×10^{-4}
M=4,500	1.62	150	45.4	1.07×10^{-13}	1.71×10^{-4}
M=10,000	1.84	112	44.2	1.13×10^{-13}	2.29×10^{-4}
M=20,000	1.92	64	37.7	1.55×10^{-13}	4.01×10^{-4}
M=100,000	1.70	106	51.6	8.26×10^{-14}	2.42×10^{-4}

The reasons for the differences can be attributed to the particle size, polarization and internal resistance of the cells. The cycling efficiencies of all samples at different cycle number are showed in Fig. 7. The first cycle irreversible capacities are 34.3, 26.4, 14.2, 9.4 and 26.3 mAh g^{-1} for the samples derived from LiPAA with mol. wt. of 2,000, 4,500, 10,000, 20,000 and 100,000, respectively.

In order to understand the influence of LiPAA with different mol. wt. on the materials in detail, electrochemical impedance spectra measurements were carried out in a fresh coin cell, as shown in Fig. 8. An intercept at the Z' axis in high frequency corresponded to the ohmic resistance (R_e), which represented the resistance of the electrolyte. The semicircle in the middle frequency range indicated the charge transfer resistance (R_{ct}). The inclined line in the low frequency represented the Warburg impedance (Z_w), which was associated with lithium-ion diffusion in the $LiFePO_4$ particles. The lithium-ion diffusion coefficient could be calculated using the following equation [33]:

$$D = R^2T^2/2A^2n^4F^4c^2\sigma^2 \quad (1)$$

where R is the gas constant, T is the absolute temperature, A is the geometric surface area of the cathode (cm^2), n is the number of electrons per molecule during oxidization, F is the Faraday constant, C is the concentration of lithium-ion (7.69×10^{-3} mol cm^{-3}) and σ is the Warburg factor which is associated with Z_{re}.

$$Z_{re} = R_e + R_{ct} + \sigma\omega^{-1/2} \quad (2)$$

where ω is frequency. Figure 9 shows the relationship plot between Z_{re} and reciprocal square root of the angular frequency ($\omega^{-1/2}$) at low-frequency region. All the parameters obtained and calculated from EIS are shown in Table 3. It can be seen that the $LiFePO_4$/C composite derived from LiPAA with mol. wt. of 20,000 has the highest exchange current density (i) and lithium-ion diffusion coefficient (which is higher than that reported in one study [39]), and the lowest R_{ct}. The exchange current density could be calculated using the following equation [34]:

$$i = RT/nFR_{ct} \quad (3)$$

It has been recognized that the middle frequency semicircle might correspond to the charge transfer impedance (R_{ct}) that resulted from the electrochemical reaction at the electrolyte and active material interface. The lower resistance of sample derived from LiPAA with mol. wt. of 20,000 can be attributed to the abundance of nano-sized microstructure on the surface of the particles, as the presence of such microstructure on the surface can aid the active material in effectively absorbing the electrolyte and thus accelerate the rate of electrochemical reaction on the interface. Meanwhile, lower polarization also can be propitious to decrease the resistance of sample. Furthermore, it is obvious that the $LiFePO_4$/C composite derived from LiPAA with mol. wt. of 20,000 has highest lithium-ion diffusion coefficient, which can be explained in terms of particle size, low polarization and resistance. Because the lithium-ion diffusion process is controlled by lithium transport across the $LiFePO_4$ | $FePO_4$ interface [35, 36]; therefore, small particle size, low polarization, and low resistance can improve the diffusion rate of lithium ion. Consequently, this enhances the performance of the $LiFePO_4$/C composite, and this is consistent with the results shown in Figs. 4, 5 and 6.

The results discussed above reveal that the mol. wt. of LiPAA is an important factor for the synthesis of $LiFePO_4$/C composite. The physical and electrochemical performances of as-prepared $LiFePO_4$/C are influenced greatly by the mol. wt. of LiPAA. When the mol. wt. of LiPAA is too small (e.g., 2,000 or 4,500), the precursor may sedimentate during drying. However, when the mol. wt. of LiPAA is too large (e.g., 100,000), the precursor will aggregate. The both extreme choice would lead to failure to synthesize $LiFePO_4$/C composite with fine particle size and electrochemical properties. The results show that LiPAA with mol. wt. of 20,000 is chosen as the optimum value for the synthesis of $LiFePO_4$/C composite.

The heating rate, synthetic temperature and sintering duration are the other three important factors that influence the electrochemical performances of $LiFePO_4$/C composite. Figure 10a shows the initial discharge capacities of as-prepared $LiFePO_4$/C composites sintered at 700 °C for 15 h with different heating rates and LiPAA with mol. wt. of 20,000. It can be seen from the figure that the maximum initial discharge capacity is reached at a

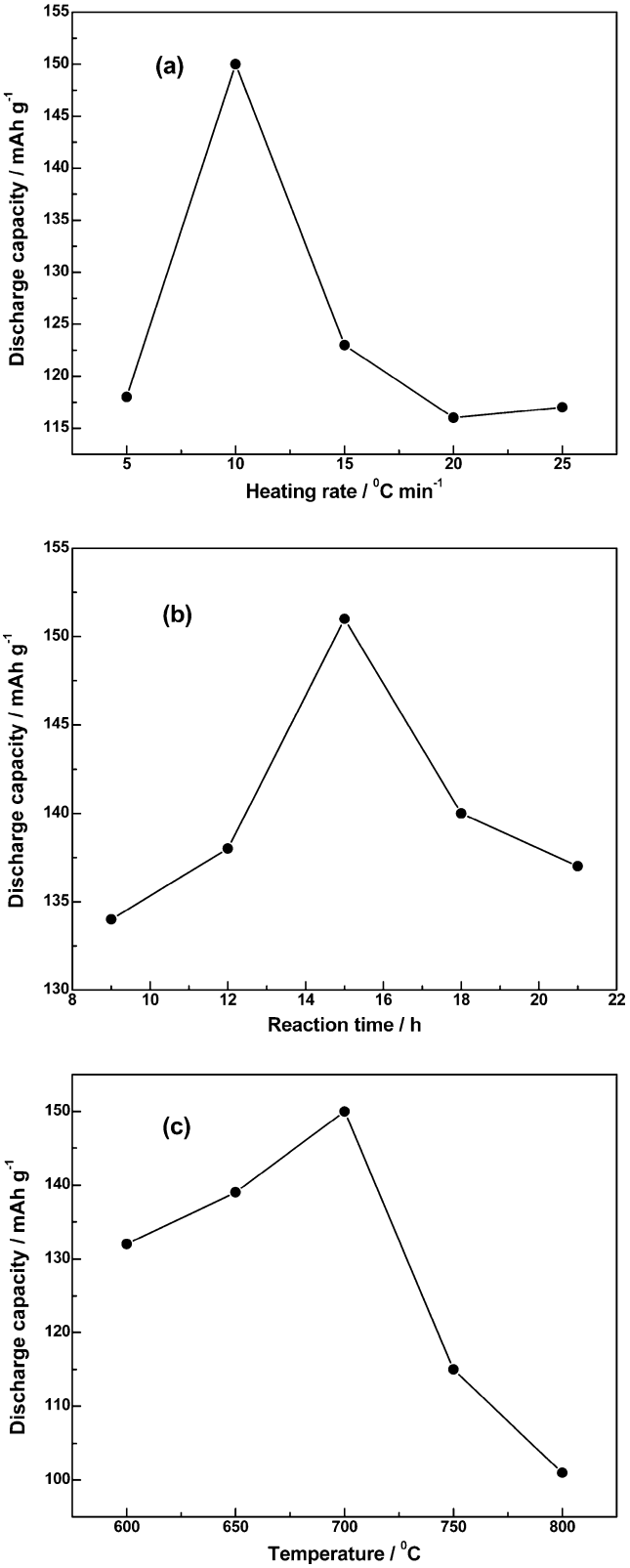

Fig. 10 Discharge capacities of $LiFePO_4$/C composites sintered under: **a** different heating rates, **b** different sintering durations, **c** different synthetic temperatures

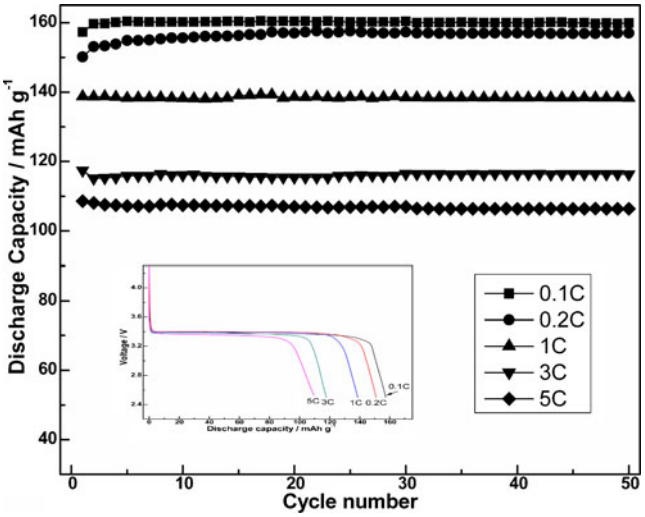

Fig. 11 Cycling performances and discharge curves of $LiFePO_4$/C composite derived from optimized synthesis conditions at various discharge rates

heating rate of 10 °C min^{-1}. The reason may be that vacancies left by small volatile molecules when heat treatment can be kept in the formed product and result in an increase of micropores. The micropores are effective places for lithium storage [37, 38]. Moreover, the interconnected microstructure helps the electrolyte to equably penetrate the electroactive materials, which leads to better electrochemical performance of $LiFePO_4$/C. At higher heating rates (>10 °C min^{-1}), the in situ pyrolyzed LiPAA form a large number of small and interconnected pores. However, excessive pores result in an increase of "dead lithium". At lower heating rates (<10 °C min^{-1}), large but separated pores are mainly formed because of small volatile molecules escaping from solid samples at lower speed, which is unfavorable for the electrolyte to equably penetrate the electroactive materials. Therefore, the heating rate of 10 °C min^{-1} is an optimum value for the synthesis of $LiFePO_4$/C.

Figure 10b reveals the initial discharge capacities of $LiFePO_4$/C composites sintered at 700 °C under different sintering durations with the heating rate of 10 °C min^{-1} and molecular weight of 20,000. As shown in Fig. 10b, the maximum initial discharge capacity is obtained at sintering duration of 15 h. It is well known that crystal integrality and granularity of products are considered as the main factors affecting the electrochemical performances. When the sintering duration is shortened, $LiFePO_4$/C with complete crystal structure may not be obtained, which leads to the instability of crystal and imposes a negative impact on the electrochemical performance of the product. When the sintering duration is increased, it is unfavorable for Li^+ diffusing in crystal due to the increase of particle size and the decrease of the specific surface area, which

Table 4 Irreversible capacity and cycling efficiency of optimized $LiFePO_4/C$ composite at different discharge rates

Discharge rates (C)	First cycle irreversible capacity (mAh g^{-1})	First cycling efficiency (%)	Second cycling efficiency (%)	Tenth cycling efficiency (%)
0.1	5.1	96.8	100.5	100.2
0.2	9.4	92.4	100.8	99.8
1	17.7	89.7	99.7	99.8
3	24.1	83.2	99.2	100
5	28.9	78.9	98.5	99.7

also affect the electrochemical performances of the product. Therefore, the sintering duration of 15 h is chosen as the optimum value for the synthesis of $LiFePO_4/C$.

The initial discharge capacities of as-prepared $LiFePO_4/C$ composites sintered for 15 h under different synthetic temperatures with the heating rate of 10 °C min^{-1} and mol. wt. of 20,000 are illustrated in Fig. 10c. It can be seen that the maximum initial discharge capacity is obtained at synthetic temperature of 700 °C. The reason for the differences also can be explained in terms of crystal integrality and granularity of products. From the above results, it can be obtained that the optimized conditions for the synthesis of $LiFePO_4/C$ composite are synthetic temperature of 700 °C, sintering duration of 15 h, heating rate of 10 °C min^{-1} and LiPAA with mol. wt. of 20,000.

Figure 11 presents the cycle performances and discharge curves (inset of Fig. 11) of as-prepared $LiFePO_4/C$ composite at the optimum conductions at various discharge rates ranging from 0.1 to 5 C. Although the discharge capacities decrease from 157 to 109 mAh g^{-1} with the increase of discharge rates from 0.1 to 5 C, the sample presents excellent capacity retention at different rates. The capacity retentions are 101.6%, 104.5%, 99.7%, 99.1% and 98% at rates of 0.1, 0.2, 1, 3 and 5, respectively, after 50 cycles. The irreversible capacities and cycling efficiencies of optimized $LiFePO_4/C$ composite at different discharge rates are listed in Table 4. The above results show that the sample prepared at optimized conditions has good rate performance and cycling stability, which can be attributed to the pyrolytic carbon derived from the LiPAA, fine particle size, low polarization and internal resistance of the cell.

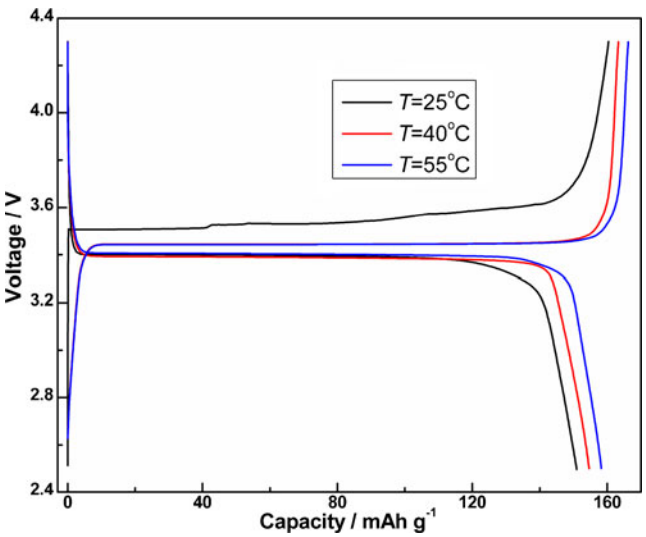

Fig. 12 The initial charge/discharge curves of optimized $LiFePO_4/C$ composites at different electrode temperatures at a rate of 0.2 C

The initial charge/discharge curves of optimized $LiFePO_4/C$ composites at different electrode temperatures are illustrated in Fig. 12. It is found that the discharge capacities of the sample increases with increasing electrode temperature. It was reported that [39] the ohmic resistance (R_e) and the charge transfer resistance (R_{ct}) decreases with the elevated electrode temperature. Moreover, from Eqs. 1 and 3, we can see that the higher the temperature, the higher the lithium-ion diffusion coefficient and exchange current density. The above reasons can also improve the electrochemistry performance of $LiFePO_4$ at elevated temperatures. From Fig. 12, we can also see that an increase in cell temperature results in a smaller voltage difference between the flat charge and discharge plateaus ($\Delta V'$), which may be attributable to low charge transfer resistance (R_{ct}) and high lithium-ion diffusion coefficient.

Conclusions

In this work, $LiFePO_4/C$ composite was obtained from LiPAA and $FePO_4{\cdot}2H_2O$ by a polymer pyrolysis reduction method. The mol. wt. of LiPAA, heating rate, synthetic temperature and sintering duration directly affected the electrochemical performance of $LiFePO_4/C$. The results demonstrate that the mol. wt. of LiPAA, heating rate, synthetic temperature and sintering duration were optimized to be 20,000, 10 °C min^{-1}, 700 °C and 15 h, respectively, at which the $LiFePO_4/C$ prevents the initial discharge capacities of 157, 139 and 109 mAh g^{-1} at rates of 0.1, 1 and 5 C, respectively, and shows the excellent cycling stability as there is no significant capacity fading after 50 cycles. Furthermore, the electrochemical performance of optimum $LiFePO_4/C$ composite at elevated temperature was also investigated.

Acknowledgements We gratefully acknowledge the support of the National High-Tech Research & Development Program of China (863 program, NO. 2009AA03Z231) and Chengdu Zhongke Laifang Energy and Technology Co. LTD.

References

1. Padhi AK, Nanjundaswamy KS, Goodenough JB (1997) J Electrochem Soc 144:1188–1194
2. Dominko R, Bele M, Goupil JM, Gaberscek M, Hanzel D, Arcon I, Jamnik J (2007) Chem Mater 19:2960–2969
3. Ellis BL, Makahnouk WRM, Makimura Y, Toghill K, Nazar LF (2007) Nat Mater 6:749–753
4. Xie HM, Wang RS, Ying JR, Zhang LY, Jalbout AF, Yu HY, Yang GL, Pan XM, Su ZM (2006) Adv Mater 18:2609–2613
5. Yang S, Song Y, Zavalij PY, Whittingham MS (2002) Electrochem Commun 4:239–244
6. Yamada A, Hosoya M, Chung SC, Kudo Y, Hinokuma K, Liu KY, Nishi Y (2003) J Power Sources 119–121:232–238
7. Dominko R, Bele M, Gaberscek M, Remskar M, Hanzel D, Goupil JM, Pejovnik S, Jamnik J (2006) J Power Sources 153:274–280
8. Wang Y, Wang Y, Hosono E, Wang K, Zhou H (2008) Angew Chem Int Ed 47:7461–7465
9. Shin HC, Park SB, Jang H, Chung KY, Cho WI (2008) Electrochim Acta 53:7946–7951
10. Chung SY, Bloking JT, Chiang YM (2002) Nat Mater 1:123–128
11. Wang D, Li H, Shi S, Huang X, Chen L (2005) Electrochim Acta 50:2955–2958
12. Wang Y, Cao G (2008) Adv Mater 20:2251–2269
13. Mi CH, Zhao XB, Cao GS, Tu JP (2005) J Electrochem Soc 152: A483–A487
14. Kim JK, Choi JW, Chauhan GS, Ahn JH, Hwang GC, Choi JB, Ahn HJ (2008) Electrochim Acta 53:8258–8264
15. Zaghib K, Shim J, Guerfi A, Charest P, Striebel KA (2005) Electrochem Solid-State Lett 8:A207–A210
16. Dominko R, Bele M, Gaberscek M, Remskar M, Hanzel D, Pejovnik S, Jamnik J (2005) J Electrochem Soc 152:A607–A610
17. Charles RS, Fausto C, Vaneica YY, Charles RM, Bruno S (2005) Electrochem Solid-State Lett 8:A484–A485
18. Cui G, Hu YS, Zhi L, Wu D, Lieberwirth I, Maier J, Müllen K (2007) Small 3:2066–2069
19. Cui G, Gu L, Zhi L, Kaskhedikar N, Aken PAV, Müllen K, Maier J (2008) Adv Mater 20:3079–3083
20. Croce F, D'Epifanio A, Hassoun J, Deptula A, Olczac T, Scrosati B (2002) Electrochem Solid-State Lett 5:A47–A50
21. Wang GX, Yang L, Chen Y, Wang JZ, Bewlay S, Liu HK (2005) Electrochim Acta 50:4649–4654
22. Fedorková A, Nacher-Alejos A, Gómez-Romero P, Oriňáková R, Kaniansky D (2010) Electrochim Acta 55:944–947
23. Huang YH, Park KS, Goodenough JB (2006) J Electrochem Soc 153:A2282–A2286
24. Park KS, Schougaard SB, Goodenough JB (2007) Adv Mater 19:848–851
25. Xia Y, Yoshio M, Noguchi H (2006) Electrochim Acta 52:240–245
26. Bauer EM, Bellitto C, Righini G, Pasquali M (2005) J Power Sources 146:544–549
27. Mestre-Aizpurua F, Hamelet S, Masquelier C, Palacín MR (2010) J Power Sources 195:6897–6901
28. Xu J, Chen G, Xie CD, Li X, Zhou YH (2008) Solid State Commun 147:443–446
29. Lai CY, Xu QJ, Ge HH, Zhou GD, Xie JY (2008) Solid State Ionics 179:1736–1737
30. Chang ZR, Lv HY, Tang HW, Li HJ, Yuan XZ, Wang HJ (2009) Electrochim Acta 54:4595–4599
31. Kadoma Y, Kim JM, Abiko K, Ohtsuki K, Ui K, Kumagai N (2010) Electrochim Acta 55:1034–1041
32. Yang KR, Lin ZJ, Hu XB, Deng ZH, Suo JS (2011) Electrochim Acta 56:2941–2946
33. Jin B, Jin EM, Park KH, Gu HB (2008) Electrochem Commun 10:1537–1540
34. Shenouda Atef Y, Murali KR (2008) J Power Sources 176:332–339
35. Churikov AV, Ivanishchev AV, Ivanishcheva IA, Sycheva VO, Khasanova NR, Antipov EV (2010) Electrochim Acta 55:2939–2950
36. Allen JL, Jow TR, Wolfenstine J (2008) J Solid State Electrochem 12:1031–1033
37. Mabuchi A, Tokumitsu K, Fujimoto H, Kasuh T (1995) J Electrochem Soc 142:1041–1046
38. Sandí G, Winans RE, Carrado KA (1996) J Electrochem Soc 143: L95–L98
39. Gao F, Tang ZY (2008) Electrochim Acta 53:5073–5075